Light-Induced Charge Separation in Anatase TiO_2 Particles

T. Berger, M. Sterrer, O. Diwald, and E. Knözinger

Institut für Materialchemie, Technical University of Vienna, A-1210 Vienna, Austria

D. Panayotov, T. L. Thompson, and J. T. Yates, Jr.*

Surface Science Center, Department of Chemistry, University of Pittsburgh, Pittsburgh, Pennsylvania 15260

Received: June 15, 2004; In Final Form: October 6, 2004

Ultraviolet light-induced electron−hole pair excitations in anatase TiO_2 powders were studied by a combination of electron paramagnetic resonance and infrared spectroscopy measurements. During continuous UV irradiation in the mW.cm^{-2} range, photogenerated electrons are either trapped at localized sites, giving paramagnetic Ti^{3+} centers, or remain in the conduction band as EPR silent species which may be observed by their IR absorption. Using low temperatures (90 K) to reduce the rate of the electron−hole recombination processes, trapped electrons and conduction band electrons exhibit lifetimes of hours. The EPR-detected holes produced by photoexcitation are O^- species, produced from lattice O^{2-} ions. It is found that under high vacuum conditions, the major fraction of photoexcited electrons remains in the conduction band. At 298 K, all stable hole and electron states are lost from TiO_2. Defect sites produced by oxygen removal during annealing of anatase TiO_2 are found to produce a Ti^{3+} EPR spectrum identical to that of trapped electrons, which originate from photoexcitation of oxidized TiO_2. Efficient electron scavenging by adsorbed O_2 at 140 K is found to produce two long-lived O_2^- surface species associated with different cation surface sites. Reduced TiO_2, produced by annealing in vacuum, has been shown to be less efficient in hole trapping than oxidized TiO_2.

I. Introduction

The light-induced production of charge carriers is the basic requirement for the application of semiconductors in photocatalysis[1−3] and photovoltaic cells.[4] Once produced, the charge carriers become trapped, either in shallow traps (ST) or in deep traps (DT), but they can also recombine, radiatively or nonradiatively, dissipating the input energy as heat. Charge carriers can react with electron donors or acceptors adsorbed on the surface of the photocatalyst.[1,2,5,6] Recombination and trapping of charge carriers accompanied by the competition with interfacial charge transfer determine the overall quantum efficiency.[1−5,7] For photocatalytic systems in which the rate-limiting step is interfacial charge transfer, improved charge separation and inhibition of charge carrier recombination is essential for enhancing the overall quantum efficiency of the photocatalytic process.[1−3,8]

Titanium dioxide, TiO_2, is the photoactive semiconductor most thoroughly investigated in the literature[1−5,7,9] because it provides the best compromise between photocatalytic performance and stability in most chemical environments; it is also inexpensive and nontoxic. Most commercial TiO_2 powdered catalysts are a mixture of rutile and anatase, and there is growing evidence which suggests that anatase is more active than rutile for oxidative detoxification reactions.[10] Anatase is the thermodynamically less stable polymorph, but the more probable phase when the TiO_2 grain size is around 10 nm as expected from surface energy calculations.[11,12] The physical and chemical properties of TiO_2 depend largely on the surface for particles a few nanometers in size.[1,12,13] This is particularly true for charge carrier trapping, because many defect states associated with the surface act as trapping sites.[1,2,14] However, on polycrystalline surfaces their exact nature and function are not well established.

X-ray absorption spectroscopy (XAS) studies[15] and electron paramagnetic resonance (EPR) spectroscopy revealed that the surface states, which trap photogenerated electrons, can be coordinatively unsaturated Ti sites formed upon reduction and surface reconstruction of TiO_2 nanoparticles. Characteristic EPR signals attributed to Ti^{3+} ions in the $g < 2$ region were observed on anatase TiO_2 samples after excitation of the solid with UV light.[16−18]

Trapping and recombination of photogenerated charge carriers have been studied by UV/vis absorption spectroscopy techniques, following transient absorption in the spectral range between the visible and the infrared region. Serpone et al.[19] and Bowman et al.[20,21] have investigated independently the primary events after band gap excitation of titanium dioxide colloids using picosecond and even sub-picosecond time resolution. Transient absorption spectra show that localization (trapping) of photogenerated electrons occurs at times below 10^{-10} s. In the larger time regime, about 10^{-9} s after the excitation pulse, more than 90% of the photogenerated charge pairs have recombined.[20,21] Bahnemann et al.[22] also observed transient UV/vis absorption following band-gap excitation of TiO_2 colloids. They assigned absorption bands centered at 1.9 and 2.8 eV to trapped electrons and holes, respectively.

Transient absorption in the IR from 3000 cm^{-1} (∼0.37 eV) to 900 cm^{-1} (∼0.15 eV) is reported for TiO_2 powders after they were exposed to UV laser pulses. This effect, attributed to photogenerated electrons in or close to the conduction band (Figure 1a), was studied by Onishi and co-workers[23] on a time scale of 5×10^{-8} s^{-1} after excitation. Lifetimes associated with decay kinetics between 10^{-7} s to 10^{-1} s were observed. In

* Corresponding author.

10.1021/jp0404293 CCC: $30.25
Published on Web 03/15/2005

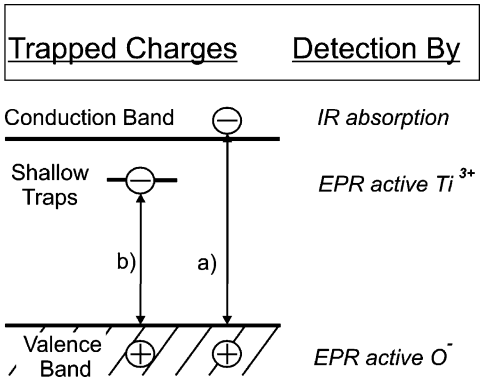

Figure 1. Scheme of UV induced charge separation in TiO_2. Electrons from the valence band can either be trapped (a) by defect states, which are located close to the conduction band (shallow traps), or (b) in the conduction band where they produce absorption in the IR region. Electron paramagnetic resonance spectroscopy detects both electrons in shallow traps, Ti^{3+}, and hole centers, O^-.

addition, an IR emission observed between 1200 and 900 cm^{-1} (0.13 eV ± 0.02 eV) occurs on a time scale of milliseconds and was attributed to the relaxation of electron−hole pairs. The above studies show that the recombination rate strongly depends on the medium in which the solid is embedded (e.g., in liquid solution or for TiO_2 dried under high vacuum conditions) and can vary by 13 orders of magnitude. [20−25]

The above examples deal with relaxation phenomena in TiO_2 (charge-carrier recombination) following laser pulse excitation. However, less direct spectroscopic information is available for photoinduced processes involving lower light irradiances, such as continuous wave excitation in the power range of mW cm^{-2}, which corresponds to the usually applied photocatalytic conditions. Hoffmann and co-workers[24] characterized the decay of free and trapped electrons in polycrystalline TiO_2 (Degussa P25) by diffuse reflectance IR spectroscopy after band gap excitation with a high-pressure Xe lamp as the UV source. After partial sample dehydroxylation, the lifetimes of these conduction band electrons are on a time scale of minutes and are controlled by the hydroxylation state of the sample. Furthermore, the infrared absorption intensity of hydroxyl stretching bands is sensitive to the electric fields caused by trapped electrons.[25] Apparently, surface hydroxyl groups actively participate in irreversible charge carrier trapping but also mediate charge recombination[5,25,26]

As indicated above, EPR is an exceptionally useful technique to probe photogenerated charge carriers in oxide particles. It allows one not only to monitor trapped electrons in localized states (Figure 1b) but also electron holes trapped at oxygen anion O^- centers which are EPR active.[15−18,27,28] In addition, adsorbed surface radicals such as superoxide anion O_2^-, formed by interfacial electron transfer from trapped electron sites to adsorbed O_2,[29] can easily be identified on the basis of their spin Hamiltonian parameters.[30] Though much is published about EPR on samples after UV exposure,[15,16,18,31−35] to the best of our knowledge nothing is known regarding the evolution of paramagnetic species in TiO_2 during continuous UV exposure and as a function of excitation time.

The objective of the present investigation is to compare, for the first time, charge trapping effects that occur during photoexcitation with supra band gap photon energy using two complementary techniques, EPR and IR spectroscopy. Whereas localized states such as holes trapped at oxygen anions (O^-) and electrons trapped at coordinatively unsaturated cations (Ti^{3+} formation) are accessible to EPR spectroscopy (Figure 1), delocalized and EPR silent electrons in the conduction band may be traced by their IR absorption that results from their electronic excitation within the conduction band in the infrared region. It will be shown that during UV excitation of anatase TiO_2 nanoparticles at 140 K and below, only a limited fraction of electrons are actually localized as Ti^{3+} states while the major fraction remains in the conduction band even after discontinuing UV excitation. The performance of these experiments under high vacuum conditions and low temperatures slows down the charge-carrier recombination and allows one to track the process of light-induced charge separation on a time scale of seconds to minutes. Moreover, after discontinuation of UV exposure, the charge separation can be stored for hours when TiO_2 particles are electronically isolated and kept at low temperatures. A comparison between photoexcitation effects on oxidized and on thermally reduced TiO_2 particles will be made, and primary interfacial charge-transfer steps that involve photogenerated electrons and O_2 (a known electron scavenger) will be addressed by this combined spectroscopic approach.

II. Experimental Section

Nanocrystalline TiO_2 particles have been produced by means of thermal decomposition of titanium isopropoxide vapor in a flow reactor system by the metal organic chemical vapor deposition (MOCVD)[36,37] method. The product powder was then gradually annealed (10 K/min) under high vacuum conditions ($p < 10^{-5}$ mbar) to 870 K, treated in vacuum for 2 h, and oxidized with 3 Torr O_2 to burn organic remnants from the precursor material. For the X-ray diffraction experiments a powder diffractometer (type XRD 3000 TT, Seifert) with monochromatic Cu Kα radiation was applied. The X-ray diffractograms were used to determine the crystalline phase and mean diameter of the particles. TEM images were taken with a 200 kV field emission gun microscope (Philipps Tecnai F20). The adsorption measurements to calculate specific surface area were performed using the BET method with N_2 at liquid nitrogen temperature.[38]

A. EPR Measurements. The EPR sample cell was made of Suprasil quartz glass and was connected to an appropriate high vacuum pumping system. It allows thermal sample activation at less than 10^{-5} Torr and UV irradiation under dynamic vacuum conditions. The EPR spectra were recorded with a Bruker EMX 10/12 spectrometer system in the X-band mode. Measurements at 90 and 140 K were performed with an ER 4131 VT variable temperature accessory. The presented spectra were obtained by accumulating 10−50 scans to guarantee sufficient signal-to-noise ratios. EPR computer simulations were performed using the SIM 14S program. The *g* values were determined on the basis of a DPPH standard.

The time evolution of electron and hole center signals were measured in situ at a fixed resonance magnetic field value for the respective EPR transitions during UV irradiation. A 300 W Xe lamp (Oriel) was used for UV irradiation. The light beam was passed through a water filter to remove IR radiation. The applied light irradiance in the energy range between 3.2 and 6.2 eV was measured with a bolometer (International Light) to be 1.4 mW cm^{-2}.

B. IR Measurements. The powdered sample was hydraulically pressed at 12000 lb/in^2 into the middle of a fine-tungsten support grid[39] as a circular spot 7 mm in diameter. The upper position on the grid is empty and is used for the background absorbance measurements in the same experiment. A type-K thermocouple is spot-welded to the top-center region of the grid. The grid is held by nickel heating and cooling supports in the

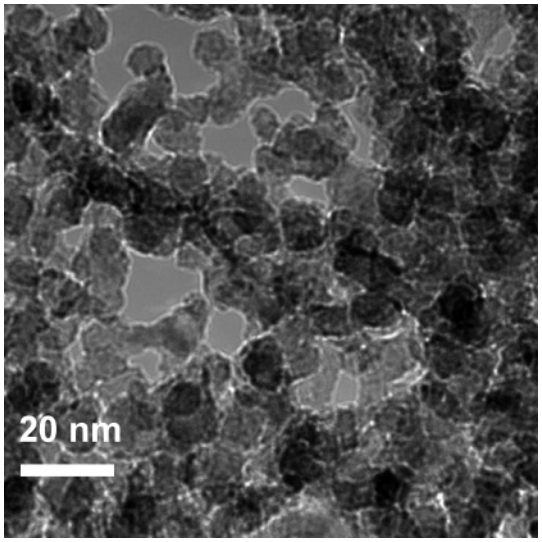

Figure 2. Transmission electron micrograph of anatase TiO_2 particles after oxidative treatment at 870 K.

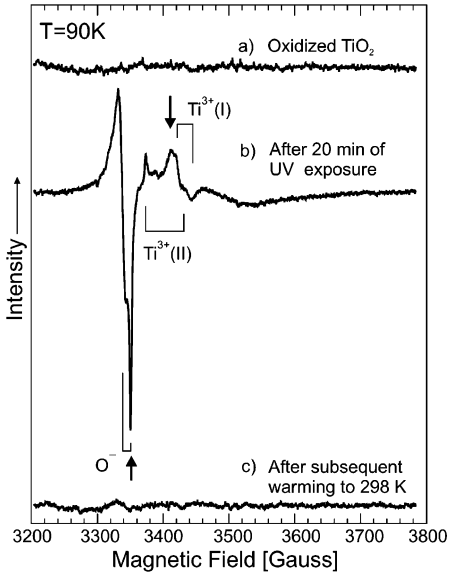

Figure 3. EPR spectra of oxidized anatase nanoparticles (a) before and (b) after 20 min of UV exposure at 90 K ($I = 1.4$ mW cm^{-2} with $h\nu > 3.2$ eV). Subsequent warming (c) to 298 K leads to the complete annihilation of paramagnetic charge carriers.

center of the dual beam IR−UV photoreactor. The grid is mounted in the cell at a 45° angle to the IR beam, so that irradiation of the grid with ultraviolet light directed perpendicularly to the IR beam can be carried out without making a geometrical change. Electrical ohmic heating and cooling with liquid nitrogen permit the temperature of the grid to be set within the range 100−1000 K. The cell gas outlet is connected to a stainless steel ultrahigh vacuum system. Both a Pfeiffer vacuum 60 L/s turbomolecular pump and a Varian 20 L/s ion pump are used to maintain the base pressure of the system below 10^{-7} Torr. A more detailed description of the IR−UV photoreactor may be found in reference 40.

For UV experiments, a 350 W high-pressure Hg arc lamp (Oriel Corp.[41]) was used as a light source. The light was filtered with a water filter to remove IR radiation. The UV light irradiance on the sample was 370 mW cm^{-2} in the energy range 3.2−6.2 eV. The infrared spectrometer was a Mattson research series I FTIR, and all scans were made in the ratio mode with a resolution of 4 cm^{-1}. Typically, 50 scans were accumulated in each spectrum. Slight heating due to IR irradiation was automatically compensated and a constant temperature of 140 K was maintained during each excitation experiment.

III. Results and Discussion

A. General Characterization of Anatase Nanoparticles. After oxidation at 870 K, the TiO_2 powder, obtained by the MOCVD method, consists of irregularly shaped TiO_2 nanoparticles with sizes between 10 and 20 nm as shown in the TEM image in Figure 2. X-ray diffraction patterns of the same powder reveal the anatase crystal structure without any trace of rutile. The mean particle diameter was determined to be 14 nm as estimated from the line width of the Bragg reflections. The specific surface area deduced from the XRD diameter value is 104 m^2 g^{-1} and corresponds reasonably to the BET adsorption measurements of 130 m^2 g^{-1}. Extensive porosity of the anatase TiO_2 material obtained by MOCVD may, therefore, be excluded.

B. Photoexcitation of Oxidized TiO_2 Nanoparticles. *1. EPR Measurements of the Photoexcitation Process.* After oxidative treatment at 870 K and cooling to 90 K, TiO_2 particles do not contain any paramagnetic sites as evidenced by a flat line shown in Figure 3a. However, after 20 min of polychromatic UV exposure ($P = 1.4$ mW cm^{-2}) at this temperature, two types of EPR features were measured (Figure 3b): a low field signal assigned to holes trapped at oxygen ions,[42−45] O^- with g tensor components at $g_\perp = 2.0121$ and $g_{||} = 2.0046$, and a second feature that is essentially composed of two distinct signals attributed to trapped electrons at Ti^{3+} sites with $g_\perp = 1.9640$ and $g_{||} = 1.9495$ (Ti^{3+} I) and $g_\perp = 1.990$ and $g_{||} = 1.9600$ (Ti^{3+} II). These values are in perfect agreement with the literature and can be readily assigned to localized electrons in anatase at different and so far unspecified sites.[17,18,30,34] EPR scans, performed at different times during UV excitation, did not reveal any additional paramagnetic signals. On the basis of these observations and in accordance with literature,[2] we specify the following charge transfer steps:

$$TiO_2 + h\nu \rightarrow e^-_{CB} + h^+_{VB} \quad (1)$$

$$e^-_{CB} + Ti^{4+} \rightarrow Ti^{3+} \text{ trapped electron} \quad (2)$$

$$h^+_{VB} + O^{2-} \rightarrow O^- \text{ trapped hole} \quad (3)$$

Whereas the injection of electrons into the conduction band and concomitantly the generation of holes in the valence band occur in femtoseconds,[2,19−21] the trapping processes of electrons (eq 2) and holes (eq 3) are observed on the time scale of seconds to minutes (Figure 4). This was carried out by tracking the intensity values at magnetic fields indicated with arrows in Figure 3b. Both curves in Figure 4 clearly show a monotonic growth within the first ∼100 s; the Ti^{3+} signal levels thereafter at a constant value,[46] while the O^- signal approaches steady state after ∼500 s. The relative ratio of Ti^{3+} and O^- signal intensities varies from sample to sample, but at 90 K, the Ti^{3+} concentration never exceeds 10% of the concentration of trapped holes. This implies that the majority of the photoexcited electrons remains in the conduction band in oxidized TiO_2. The persistent filling of the conduction band with electrons is in line with photoconductivity measurements performed on TiO_2 powders upon excitation with comparable light irradiances.[47,48]

Discontinuation of UV excitation after 1200 s results in signal depletion to about 90% of the maximum intensity achieved during irradiation for O^- and 50% for the Ti^{3+} signals, as shown in Figure 4. Then, the signals remain constant on a time scale

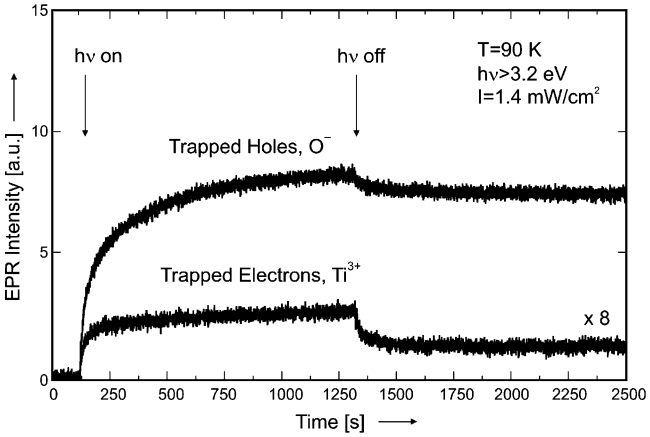

Figure 4. Concentration of O^- and Ti^{3+} centers as a function of UV exposure time ($I = 1.4$ mW cm^{-2} with $h\nu > 3.2$ eV).

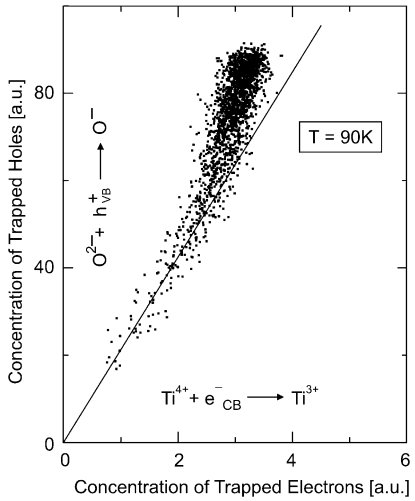

Figure 5. Correlation of O^- and Ti^{3+} EPR signal intensity as a function of UV exposure time at 90 K ($I = 1.4$ mW cm^{-2} with $h\nu > 3.2$ eV). The intensity values for the Ti^{3+} and O^- species were normalized with respect to equal integral intensities of the respective spin center signals.

of hours (no significant signal decrease was observed after 5 h of sample storage at 90 K). To characterize the correlation between hole and electron centers, the O^- concentration was plotted against the Ti^{3+} concentration as UV exposure time increases at 90 K (Figure 5). The significant deviation from linearity at higher spin concentrations suggests that only a limited number of photoexcited and trapped electrons occupy localized states (Figure 1b). A considerable fraction must remain in the conduction band as delocalized and EPR silent species[24,25,47,48] (Figure 1a).

Light-induced filling of the conduction band with electrons is the exclusive process observed when the experiment is performed at temperatures somewhat higher than 90 K: no Ti^{3+} centers were observed during photoexcitation at 140 K, even after subsequent cooling to 90 K. Although the O^- signal (not shown) obtained at 140 K is lower in intensity, it follows essentially the same kinetics as in the experiment performed at 90 K. Because the relative Ti^{3+} concentration has a significant dependence on temperature between 90 and 140 K, activation energies around 0.01 eV are estimated for the process of diffusion of shallowly trapped electrons from their Ti^{3+} trapping sites, followed by recombination with holes. Sample excitation at 298 K does not produce any paramagnetic states at all. Also, raising the temperature to 298 K after UV excitation at 90 K (Figure 3c) results in the complete annihilation of photogenerated charges.

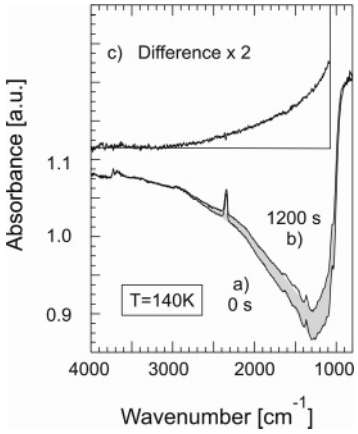

Figure 6. IR spectra of oxidized anatase TiO_2 particles at 140 K: (a) before and (b) after 20 min of UV exposure. The inset (c) represents the difference (b−a).

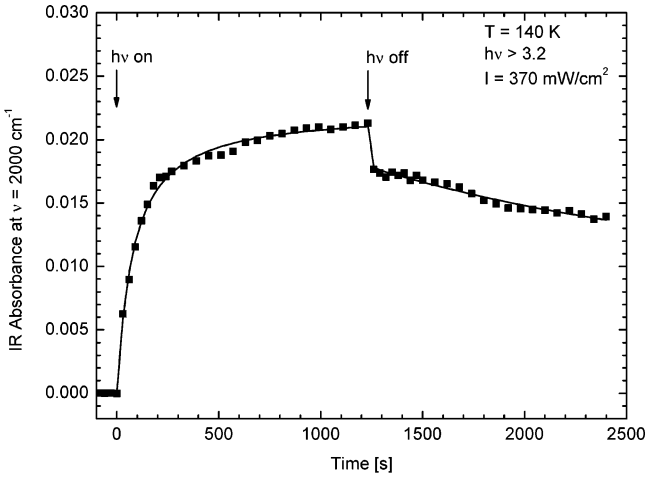

Figure 7. Time-resolved IR absorbance at 2000 cm^{-1} during and after UV exposure at 140 K.

2. IR Measurements of the Photoexcitation Process. Illumination of oxidized TiO_2 particles with polychromatic UV light (3.2 eV− 6.2 eV, $P = 370$ mW cm^{-2}) at 140 K in vacuum causes a pronounced increase in the background IR absorbance over the entire region from 3000 to 1000 cm^{-1} as the UV exposure time increases (Figure 6a,b). Subtraction of the spectrum before the beginning of irradiation (Figure 6a) from the excited state spectrum (Figure 6b) produces a structureless broad IR absorption background feature, monotonically strengthened with decreasing wavenumber from 3000 to 1000 cm^{-1} (Figure 6c). The spectrum 6c was ratioed to the spectrum of an empty tungsten grid under the same conditions of illumination to exclude possible background effects originating from the grid. The spectral shape of the background feature (Figure 6c) does not change with UV exposure time. To track signal changes as a function of UV exposure, IR spectra were acquired every 30 s and a representative absorbance value at 2000 cm^{-1} was plotted against irradiation time. Figure 7 presents the IR signal changes obtained at 140 K in vacuum during the illumination and dark periods. The resulting profile qualitatively corresponds to the excitation curve measured by EPR for the evolution of O^-. Upon discontinuing the UV exposure, the IR signal continuously decreases.

This type of broad and structureless IR absorption has been reported by several authors for TiO_2 after UV excitation.[23−25,49−51] According to Yamakata et al.,[23,49] photogenerated electrons trapped in shallow gap states are the source of the transient IR

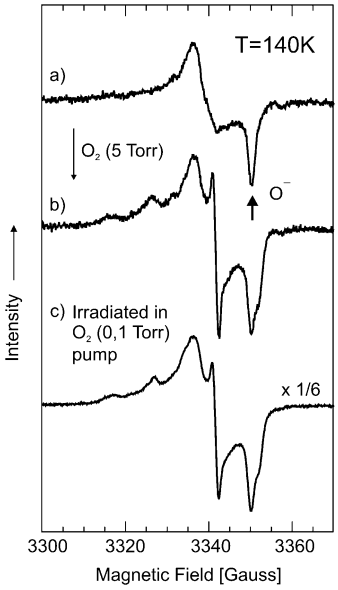

Figure 8. (a) EPR spectra of oxidized anatase TiO_2 particles after 20 min UV exposure at 140 K; (b) after exposure to 5 mbar O_2 followed by evacuation; (c) the spectrum was measured after 20 min UV exposure at 140 K in the presence of O_2.

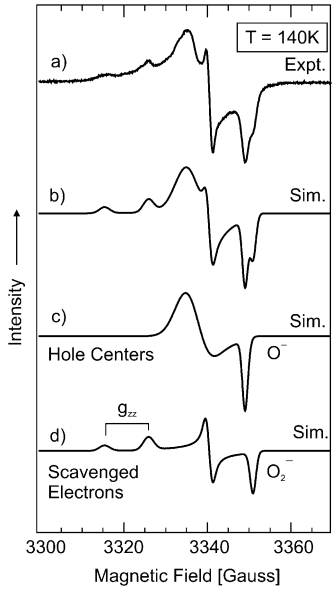

Figure 9. (a) Experimental EPR spectrum after 20 min UV exposure at 140 K, (from Figure 8c); (b) the simulation result. Figures 9c and d display the simulated O^- and O_2^- components of spectrum (b), respectively.

absorption via two routes: the intra-CB transition of free electrons thermally excited from the trap state, and the direct optical transition from the trap state to the CB. Szczepankiewicz et al. have recently shown[25] that, during illumination of TiO_2 surfaces under vacuum, the electron trapping and annihilation is slowed such that the free electrons, typically monitored by ultrafast techniques,[2,19−23] maintain an unusually long lifetime of minutes to hours. Complementary to the EPR results of this study, where no paramagnetic electron states were observed after excitation at 140 K, we demonstrate that a continuous IR absorption points to the presence of electrons in the conduction band which are kept separated from their complementary holes even after discontinuation of UV exposure. A possible explanation for such a persistent storage of electrons comes from Emeline et al.:[52] because the translation symmetry in spatially confined nanoparticles is valid only for the short-length crystal units, the number of states forming the band states is very limited compared to a bulk crystal. As a consequence, the communication between different states in the conduction band is much less effective and the decay of electrons can be significantly delayed. When the TiO_2 temperature was raised to 298 K (not shown in Figure 7), the slowly decaying IR absorption immediately decreased to a level close to the original baseline. As in the corresponding EPR experiment (Figure 3c) charge carrier separation was reversed via thermally induced charge carrier recombination.

C. The Effect of Oxygen Adsorption on Charge Separation. *1. EPR Measurements of the Effect of O_2.* To elucidate the effect oxygen has on both trapped electrons and on the process of electron trapping, the following EPR experiments were performed at 140 K. UV exposure in vacuum was found to produce paramagnetic hole centers exclusively (O^- radicals, Figure 8a); centers due to Ti^{3+} have recombined with O^- holes at 140 K. Contacting the pre-irradiated powder with 5 Torr O_2 in the dark followed by evacuation leads to significant changes in the spectrum (Figure 8b). Photoexcitation of TiO_2 nanoparticles in the presence of oxygen at the same temperature and subsequent evacuation (Figure 8c) produces essentially the same result as observed for O_2 addition to pre-irradiated TiO_2 (Figure 8b). However, the overall intensity is enhanced by a factor of 6 when irradiation occurs in the presence of O_2.

TABLE 1: Parameters of the *g* Matrix for Paramagnetic Species Isolated on Anatase TiO_2 Particles

trapped holes O^-			
	$g_\perp = 2.0121$	$g_\parallel = 2.0046$	
scavenged electrons O_2^-			
O_2^- [I]	$g_{zz} = 2.0248$	$g_{yy} = 2.0096$	$g_{xx} = 2.0033$
O_2^- [II]	$g_{zz} = 2.0184$	$g_{yy} = 2.0096$	$g_{xx} = 2.0033$
trapped electrons - Ti^{3+}			
Ti^{3+} [I]	$g_\perp = 1.9640$	$g_\parallel = 1.9495$	
Ti^{3+} [II]	$g_\perp = 1.9900$	$g_\parallel = 1.9600$	
background			
	$g_{iso} = 1.9300$		

To understand the spectral lines observed in Figure 8b and c as a result of the presence of O_2, a simulation was performed as shown in Figure 9. Two or more oxygen-centered radical species are found. The results of the best fit are given in Figure 9b, and the *g* values corresponding to the paramagnetic species are listed in Table 1. In addition to O^- (Figure 9c), a set of three additional component features (Figure 9d) contribute to the total spectrum. The associated *g* values are easily assigned to adsorbed superoxy species O_2^-.[28,30,45,53] In EPR applied to the investigation of oxide surfaces, this type of oxygen radical is a widely used probe for cationic surface sites because it has specific resonances within the low field region (g_{zz}), indicative of the local crystal fields at the respective O_2^- adsorption sites.[53] In the present case, two different surface cations serve as adsorption sites for the newly formed oxygen radicals as evidenced by their resonances at $g_{zz} = 2.025$ and $g_{zz} = 2.018$ (Figure 9a and d).

To summarize, the effect of oxygen on light-induced charge separation at temperatures $T > 90$ K can be described by an interfacial transfer of electrons out of both localized paramagnetic states and the conduction band to molecular oxygen by eqs 4 and 5:

$$Ti^{3+} + O_2 \rightarrow Ti^{4+} \cdots O_2^- \text{ (not shown)} \qquad (4)$$

$$Ti^{4+} + e^-_{CB} + O_2 \rightarrow Ti^{4+} \cdots O_2^- \qquad (5)$$

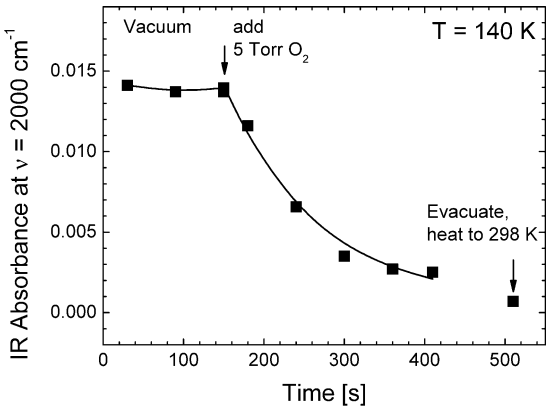

Figure 10. IR background intensity at 2000 cm^{-1} of irradiated oxidized anatase TiO_2 particles upon addition of O_2 at 140 K.

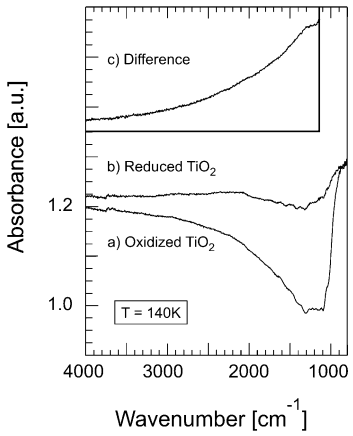

Figure 11. Comparison of background IR behavior of (a) oxidized TiO_2 and (b) reduced TiO_2 at 140 K.

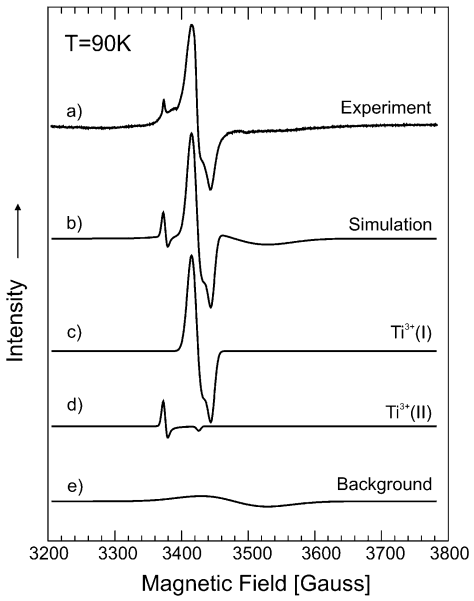

Figure 12. EPR spectra of oxidized TiO_2 at 90 K.

These reactions are exothermic (−42 kJ/mol) and additionally are favored by Coulombic stabilization of the lattice.[30]

Simulation of the superimposed feature in Figure 9a,b into its O^- (Figure 9c) and O_2^- related signals (Figure 9d) reveals comparable intensities of O^-/O_2^- of ∼1.1:1 and, thus, an equal concentration of holes trapped by lattice O^{2-} to produce O^-, and electrons scavenged by molecular oxygen. This is true for O_2 addition to pre-irradiated TiO_2 in the dark (Figure 8b) as well as for UV excitation in the presence of O_2 (Figure 8c). When photogenerated electrons are trapped by adsorbed O_2 species, the state of charge separation can be maintained even after warming to room temperature. The clear proportionality between trapped holes (O^-) and scavenged electrons (O_2^-) and the lack of other oxygen adducts such as $O^-...O_2$ as reported by others[45] point to the fact that even under UV exposure the O_2^- species remain on the surface as undissociated species.

A comparison of the O_2^- EPR intensities for O_2 post addition to irradiated TiO_2 with TiO_2 irradiated in the presence of O_2(g) shows that the presence of O_2(g) produces a 6-fold enhancement of the O_2^- surface concentration. The fraction of the long-lived trapped charges, which are transferred to post-adsorbed O_2 is ∼17% as judged by the O_2 titration experiment. When O_2(g) is continuously supplied to the interface during irradiation in O_2(g), an additional ∼83% of O_2^- is produced as all photoexcited electrons are transferred to O_2. In both experiments, the two O_2^- species are produced in the same ratio.

2. IR Measurements of the Effect of O_2. Figure 10 shows the effect of adding O_2 (5 Torr) to the irradiated TiO_2 surface at 140 K using the intensity of the IR background at 2000 cm^{-1} as a detector for trapped conduction band electrons. The experiment is similar to the 140 K EPR experiment of Figure 8a,b. The decrease in IR absorbance at 2000 cm^{-1} indicates that O_2 efficiently removes long-lived trapped electron charge in the conduction band produced by UV excitation of TiO_2 in vacuum. Warming to 298 K results in a small additional removal of trapped electron charge, possibly by activated recombination.

D. Photoexcitation of Reduced TiO_2 Nanoparticles. Thermal treatment of TiO_2 nanoparticles in vacuum (<10^{-5} Torr) and at 950 K produces an intense blue color as the reduced solid is produced. The optical absorption in the range of visible light is accompanied by a pronounced increase in the background absorbance in the mid-IR region (Figure 11b) compared to oxidized TiO_2 powder. As in the case of oxidized TiO_2 under UV excitation (Figure 6c), the increased background (Figure 11c) must be attributed to the production of conduction band electrons that absorb IR light.[23−25,50] For reduced TiO_2 produced by vacuum annealing, this profound change in the electronic structure is caused by the loss of lattice oxygen anions via desorption of molecular O_2 during thermal treatment.

IR measurements of the level of background absorbance during UV exposure of reduced anatase TiO_2 showed no change. After UV exposure the observed background absorbance was identical to that shown in Figure 11c. Also increasing the temperature to 298 K did not produce any effect.

A typical EPR spectrum of reduced anatase TiO_2 particles, shown in Figure 12a, contains essentially the same Ti^{3+} related signals (Figure 12c and d) as observed for Ti^{3+} states in oxidized TiO_2 produced by UV excitation (Figure 3b, Table 1). The spin concentration is, however, by a factor of 25 higher for reduced TiO_2. Upon 20 min light exposure with 1.4 mW cm^{-2}, the signal intensity does not change (Figure 13a and b) and only traces of O^- hole center signals corresponding to less than 5% of the concentration measured on oxidized TiO_2 appear. These small EPR signals completely vanish after discontinuation of light exposure (Figure 13b). The absence of trapped holes in reduced TiO_2 could be related to the deficiency of lattice oxygen trapping sites and/ or the already high concentration of electrons in excited states, either localized or delocalized (band filling mechanism).[51,54]

When higher light irradiances (> 5 mW/cm^2) are applied to reduced TiO_2, the Ti^{3+} centers also disappear (not shown). This bleaching process occurs already with photons of energy below

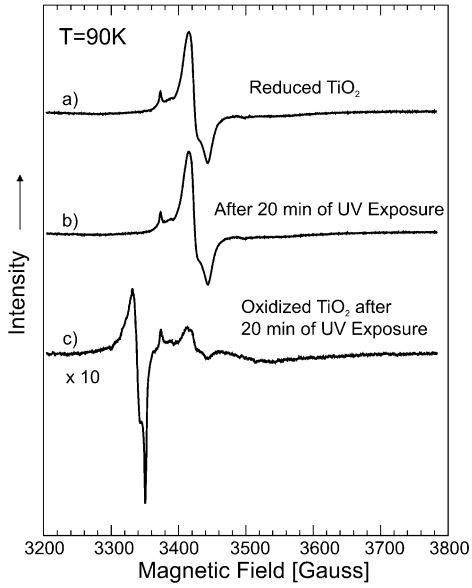

Figure 13. The effect of UV irradiation on trapped electrons in reduced TiO_2 at 90 K.

1.6 eV and indicates that the electronic states due to trapped electrons (Ti^{3+}) are located within the band gap and can be ionized with significantly lower photon energies than are required for electron−hole pair excitation across the 3.2 eV band gap. Similar observations were made in an earlier study by Servicka et al.[32] In addition, Ghosh et al.[55] observed the presence of eight specific levels less than 1 eV below the conduction band. They speculated that these levels may be associated with Ti^{3+} ions at regular and interstitial sites and with color centers. Gravelle et al.[56] tentatively assigned two Ti^{3+} ions to regular and interstitial lattice positions.

In addition, for reduced TiO_2, the Ti^{3+} signal in Figure 12a as well as the optical absorptions in the visible and the mid-IR are observed to disappear with O_2 exposure, producing the O_2^- ESR signal as expected from O_2 electron scavenging. These conclusions must be considered in connection with recent work where it was proposed that self-doping of anatase, by making it substoichimetric and producing large concentrations of Ti^{3+} sites, would lead to visible light activity for the degradation of pollutants.[57,58] Since these photocatalytic reactions are usually carried in the presence of oxygen which would oxidize the electronically reduced particles, a persistent visible activity is unlikely.

E. Electrical Conduction Effects in Photochemistry Experiments − An Hypothesis based on a Comparison of ESR and IR Studies. The TiO_2 powder, and its pretreatment, in the EPR and the IR experiments, was identical. To avoid warming of the EPR samples, the UV radiation power was maintained at 1.4 mW cm^{-2}, whereas the IR experiments involved UV power of 370 mW cm^{-2}. In the case of the EPR experiments, the TiO_2 is loosely contained in a quartz tube and electrically isolated from ground, whereas, for the IR measurements, the TiO_2 is compressed into a tungsten mesh support which is in electrical contact with ground. The two different support methods are associated with different production and decay rates for the trapped charges. In the EPR experiments, the concentration of trapped holes and trapped electrons remained essentially constant for hours after irradiation was discontinued, whereas in the IR experiments, the trapped conduction-band electrons exhibited a monotonic loss of concentration after the UV radiation was discontinued. The difference in decay kinetics and in power levels required in the two experiments are postulated to be due to the different degrees of electrical isolation of the TiO_2 particles in the two experiments.

IV. Conclusions

The following conclusions have been reached in this work: (1) Photogenerated electrons and holes are produced by band gap UV radiation on powdered anatase TiO_2. Trapped holes are detected as O^- species, generated from lattice O^{2-} in the valence band. The electrons are detected either as Ti^{3+} species or as electrons captured in the conduction band. (2) At 90 K, both electrons and holes are trapped for hours. (3) At 140 K, Ti^{3+} trapped electron states can recombine with holes, whereas conduction band electrons are stable. (4) At 298 K, all stable trapped hole and trapped electron states are lost from TiO_2. (5) The major fraction of photoexcited electrons remain in the conduction band, rather than being trapped as Ti^{3+} states. (6) The presence of O_2 during excitation at 140 K leads to the formation of two long-lived superoxy O_2^- states associated with different titanium cation sites on the surface. (7) Defect sites (Ti^{3+}) produced by annealing TiO_2 are identical to the Ti^{3+} sites produced by photoexcitation. (8) The photoproduction of stable hole states in reduced TiO_2 is found to be very inefficient compared to those photoproduced in oxidized TiO_2.

Acknowledgment. The Vienna group acknowledges gratefully the support of the Austrian Science Foundation (Contract numbers J2058 and P 14731-CHE). T.B. would like to thank the Österreichische Forschungsgemeinschaft for financially contributing to his stay at the Surface Science Center in Pittsburgh. We thank Scott D. Walck for his assistance with TEM measurements. We acknowledge with thanks the support of this work by the DARPA DoD Multidisciplinary University Research Initiative (MURI) program administered by the Army Research Office under Grant DAAD 19-01-0-0619.

References and Notes

(1) Linsebigler, A. L.; Lu, G. Q.; Yates, J. T., Jr. *Chem. Rev.* **1995**, *95*, 735−758.
(2) Hoffmann, M. R.; Martin, S. T.; Choi, W. Y.; Bahnemann, D. W. *Chem. Rev.* **1995**, *95*, 69−96.
(3) Serpone, N.; Pilezzetti, E. *Photocatalysis: Fundamentals and Applications*; Wiley-Interscience: New York, 1989.
(4) Kalayanasundaram, K.; Gratzel, M. *Coord. Chem. Rev.* **1998**, *77*, 347−414.
(5) Henderson, M. A.; Epling, W. S.; Peden, C. H. F.; Perkins, C. L. *J. Phys. Chem. B* **2003**, *107*, 534−545.
(6) Panayotov, D.; Yates, J. T., Jr. *Chem. Phys. Lett.* **2003**, *381*, 154−162.
(7) Peral, J.; Domenech, X.; Ollis, D. F. *J. Chem. Technol. Biotechnol.* **1997**, *70*, 117−140.
(8) Bedja, I.; Kamat, P. V. *J. Phys. Chem.* **1995**, *99*, 9182−9188.
(9) Howe, R. F. *Dev. Chem. Eng. Mineral Process* **1998**, *6*, 55−85.
(10) Bahnemann, D. W.; Bockelemann, D.; Goslich, R.; Hilgendorff, M.; Weichgrebe, D. *Photocatalytic Purification and Treatment of Water and Air*; Elsevier Science Publishers: Amsterdam, 1993.
(11) Gribb, A. A.; Banfield, J. F. *Am. Mineral* **1997**, *82*, 717−728.
(12) Diebold, U.; Ruzycki, N.; Herman, G. S.; Selloni, A. *Catal. Today* **2003**, *85*, 93−100.
(13) Beydoun, D.; Amal, R.; Low, G.; McEvoy, S. *J. Nanoparticle Res.* **1999**, *1*, 439−458.
(14) Diebold, U. *Surf. Sci. Rep.* **2003**, *48*, 53−229.
(15) Chen, L. X.; Rajh, T.; Wang, Z. Y.; Thurnauer, M. C. *J. Phys. Chem. B* **1997**, *101*, 10688−10697.
(16) Hurum, D. C.; Agrios, A. G.; Gray, K. A.; Rajh, T.; Thurnauer, M. C. *J. Phys. Chem. B* **2003**, *107*, 4545−4549.
(17) Meriaudeau, P.; Che, M.; Gravelle, P. C.; Teichner, S. *Bull. Soc. Chim. France* **1971**, *1*, 13−22.
(18) Rajh, T.; Makarova, O. V.; Thurnauer, M. C.; Cropek, D. In *Synthesis, Functionalization and Surface Treatment of Nanoparticles*; Baraton, M. I., Ed.; American Science Publishers: Stevenson Ranch, CA, 2003.
(19) Serpone, N.; Lawless, D.; Khairutdinov, R.; Pelizzetti, E. *J. Phys. Chem.* **1995**, *99*, 16655−16661.

(20) Colombo, D. P.; Bowman, R. M. *J. Phys. Chem.* **1995**, *99*, 11752−11756.
(21) Colombo, D. P.; Bowman, R. M. *J. Phys. Chem.* **1996**, *100*, 18445−18449.
(22) Bahnemann, D. W.; Hilgendorff, M.; Memming, R. *J. Phys. Chem. B* **1997**, *101*, 4265−4275.
(23) Yamakata, A.; Ishibashi, T.; Onishi, H. *Chem. Phys. Lett.* **2001**, *333*, 271−277.
(24) Szczepankiewicz, S. H.; Moss, J. A.; Hoffmann, M. R. *J. Phys. Chem. B* **2002**, *106*, 2922−2927.
(25) Szczepankiewicz, S. H.; Moss, J. A.; Hoffmann, M. R. *J. Phys. Chem. B* **2002**, *106*, 7654−7658.
(26) Henderson, M. A.; White, J. M.; Uetsuka, H.; Onishi, H. *J. Am. Chem. Soc.* **2003**, *125*, 14974−14975.
(27) Diwald, O.; Sterrer, M.; Knözinger, E.; Sushko, P. V.; Shluger, A. L. *J. Chem. Phys.* **2002**, *116*, 1707−1712.
(28) Sterrer, M.; Diwald, O.; Knözinger, E. *J. Phys. Chem. B* **2000**, *104*, 3601−3607.
(29) Emeline, A. V.; Smirnova, L. G.; Kuzmin, G. N.; Basov, L. L.; Serpone, N. *Photochem. Photobiol. A: Chemistry* **2002**, *148*, 97−102.
(30) Attwood, A. L.; Murphy, D. M.; Edwards, J. L.; Egerton, T. A.; Harrison, R. W. *Res. Chem. Intermed.* **2003**, *29*, 449−465.
(31) Riegel, G.; Bolton, J. R. *J. Phys. Chem.* **1995**, *99*, 4215−4224.
(32) Servicka, E.; Schlierkamp, M. W.; Schindler, R. N. *Z. Nanoforsch.* **1981**, *36a*, 226−232.
(33) Anpo, M.; Che, M.; Fubini, B.; Garrone, E.; Giamello, E.; Paganini, M. C. *Top. Catal.* **1999**, *8*, 189−198.
(34) Howe, R. F.; Gratzel, M. *J. Phys. Chem.* **1987**, *91*, 3906−3909.
(35) Jenkins, C. A.; Murphy, D. M. *J. Phys. Chem. B* **1999**, *103*, 1019−1026.
(36) Benfer, S.; Knözinger, E. *J. Mater. Chem.* **1999**, *9*, 1203−1209.
(37) Schleich, D. M.; Walter, B. *Nanostruct. Mater.* **1997**, *8*, 579−586.
(38) Brunauer, S.; Emmett, P. H.; Teller, E. *J. Am. Chem. Soc.* **1938**, *60*, 309−319.
(39) Ballinger, T. H.; Wong, J. C. S.; Yates, J. T., Jr. *Langmuir* **1992**, *8*, 1676−1678.
(40) Wong, J. C. S.; Linsebigler, A.; Lu, G. Q.; Fan, J. F.; Yates, J. T., Jr. *J. Phys. Chem.* **1995**, *99*, 335−344.
(41) *The Book of Photon Tools*; Oriel Corporation.
(42) Micic, O. I.; Zhang, Y. N.; Cromack, K. R.; Trifunac, A. D.; Thurnauer, M. C. *J. Phys. Chem.* **1993**, *97*, 7277−7283.
(43) Sterrer, M.; Diwald, O.; Knözinger, E.; Sushko, P. V.; Shluger, A. L. *J. Phys. Chem. B* **2002**, *106*, 12478−12482.
(44) Che, M.; Tench, A. J. *Adv. Catal.* **1982**, *31*, 78−148.
(45) Volodin, A. M.; Chercashin, A. E.; Zakharenko, V. S. *React. Kinet. Catal. Lett.* **1979**, *11*, 103−106.
(46) That only a monotonic increase in the Ti^{3+} signal is observed in the course of UV exposure time, indicates that a second light-induced electron-transfer step: $Ti^{3+} + e^- = Ti^{2+}$ does not occur in the course of continuous UV exposure.
(47) Herrmann, J.-M.; Disdier, J.; Pichat, P. *J. Chem. Soc., Faraday Trans. I* **1981**, *77*, 2815−2826.
(48) Nelson, J.; Eppler, A.; Ballard, I. M. *Photochem. Photobiol. A: Chemistry* **2002**, *148* 25−31.
(49) Yamakata, A.; Ishibashi, T.; Onishi, H. *J. Mol. Catal. A-Chem.* **2003**, *199*, 85−94.
(50) Pankove, J. I. *Optical Processes in Semiconductors*; Dover: New York, 1975.
(51) Basu, P. K. *Theory of Optical Processes in Semiconductors*; Oxford University Press: New York, 1997.
(52) Emeline, A.; Salinaro, A.; Serpone, N. *J. Phys. Chem. B* **2000**, *104*, 11202−11210.
(53) Che, M.; Tench, A. J. *Adv. Catal.* **1983**, *32*, 2−148.
(54) Liu, C.-Y.; Bard, A. J. *J. Phys. Chem.* **1989**, *93*, 3232−3237.
(55) Ghosh, A. K.; Wakim, F. G.; Adiss, P. R. *Phys. Rev.* **1969**, *184*, 979−988.
(56) Gravelle, P. C.; Juillet, F.; Meriaudeau, P.; Teichner, S. *Faraday Discuss. Chem. Soc.* **1971**, *52*, 140−148.
(57) Justicia, I.; Ordejon, P.; Canto, G.; Mozos, J. L.; Fraxedas, J.; Battiston, G. A.; Gerbasi, R.; Figueras, A. *Adv. Mater.* **2002**, *14*, 1399−1402.
(58) Nakamura, I.; Negishi, N.; Kutsuna, S.; Ihara, T.; Sugihara, S.; Takeuchi, E. *J. Mol. Catal. A-Chem.* **2000**, *161*, 205−212.